Front. Phys. 13(4), 136401 (2018)
https://doi.org/10.1007/s11467-018-0751-9

RESEARCH ARTICLE

Analytical approach to quantum phase transitions of ultracold Bose gases in bipartite optical lattices using the generalized Green's function method

Zhi Lin[1,2,†], **Jun Zhang**[2], **Ying Jiang**[2,3,4]

[1] *Department of Physics, State Key Laboratory of Surface Physics and Laboratory of Advanced Materials, Fudan University, Shanghai 200433, China*
[2] *Department of Physics, Shanghai University, Shanghai 200444, China*
[3] *Qian Weichang College, Shanghai University, Shanghai 200444, China*
[4] *Key Lab for Astrophysics, Shanghai 200234, China*
Corresponding author. E-mail: [†] *zhilin13@fudan.edu.cn*
Received September 11, 2017; accepted November 30, 2017

In order to investigate the quantum phase transitions and the time-of-flight absorption pictures analytically in a systematic way for ultracold Bose gases in bipartite optical lattices, we present a generalized Green's function method. Utilizing this method, we study the quantum phase transitions of ultracold Bose gases in two types of bipartite optical lattices, i.e., a hexagonal lattice with normal Bose–Hubbard interaction and a d-dimensional hypercubic optical lattice with extended Bose–Hubbard interaction. Furthermore, the time-of-flight absorption pictures of ultracold Bose gases in these two types of lattices are also calculated analytically. In hexagonal lattice, the time-of-flight interference patterns of ultracold Bose gases obtained by our analytical method are in good qualitative agreement with the experimental results of Soltan-Panahi, *et al.* [*Nat. Phys.* 7, 434 (2011)]. In square optical lattice, the emergence of peaks at $(\pm\frac{\pi}{a}, \pm\frac{\pi}{a})$ in the time-of-flight absorption pictures, which is believed to be a sort of evidence of the existence of a supersolid phase, is clearly seen when the system enters the compressible phase from charge-density-wave phase.

Keywords ultracold Bose gases, quantum phase transition, bipartite optical lattice, generalized Green's function method, time-of-flight absorption picture

PACS numbers 03.75.Hh, 64.70.Tg, 67.85.Hj, 03.75.Lm

1 Introduction

Without any doubt, the physics of ultracold Bose gases in optical lattices has become one of the hottest research fields for more than a decade [1] due to their novelties and various potential applications as so-called quantum simulations [2, 3]. Among the research topics on ultracold Bose gases in optical lattices, to determine the ground states and the corresponding quantum phase transitions [4] is one of the major problems [1, 5, 6].

As is well known [6], ultracold spinless Bose gases in a homogeneous optical lattice can be described by the elegant Bose–Hubbard Hamiltonian [3, 5]

$$\hat{H}_{\mathrm{BH}} = \hat{H}_1 + \hat{H}_0 \tag{1}$$

with the diagonal part $\hat{H}_0$ and the hopping part $\hat{H}_1$ being

$$\hat{H}_0 = \sum_i \left[\frac{U}{2}\hat{n}_i(\hat{n}_i - 1) - \mu\hat{n}_i\right],$$
$$\hat{H}_1 = -J\sum_{\langle i,j\rangle} \hat{a}_i^\dagger \hat{a}_j, \tag{2}$$

respectively. Here $\hat{n}_i = \hat{a}_i^\dagger \hat{a}_i$ is the particle number operator on i-th site, J is the hopping amplitude of the bosons between the nearest-neighbor sites i and j, U denotes the on-site repulsion, and μ is the chemical potential. To investigate this simple yet nontrivial Hamiltonian analytically, mean field theory [5] and strong-coupling expansion [7] can be employed. However, comparisons with the Monte Carlo simulation results [8] show that the former underestimates the phase boundary while the latter goes in the opposite direction [9].

*arXiv: 1402.3925.

Based on the effective potential and Rayleigh-Schrödinger perturbation theory, treating the hopping parameter as a perturbation, an alternative analytical approach has been developed [9]. With this novel systematic approach, the superfluid-Mott-insulator(SF-MI) quantum phase boundaries of ultracold Bose gases in square and cubic lattices [9] as well as in non-rectangular optical lattices (including triangular, hexagonal, and Kagomé lattices) [10] have been calculated analytically, in good agreement with the numerical results [11] obtained by a high-order hopping expansion of the effective potential method [9].

The above-mentioned effective potential method can only be used to calculate the quantum phase boundaries. Instead, Green's function can not only indicate the location of second-order phase transition boundaries by its divergence [12, 13], but also reveal the information of the distribution function of the system [14]. The latter can be detected directly in experiment via time-of-flight technique [1, 3]. In cubic lattice, time-of-flight absorbtion pictures and the corresponding visibility have been presented by Green's function via a strong-coupling calculation [15], however, these results cannot be compared with the experimental data due to ghost peaks in calculation [16]. Hence, an new analytical systematic approach (re-summed Green's function method) have been developed [16–18]. Based on the same perturbation treatment as in the effective potential theory, utilizing the cumulants expansion and re-summed Green's function technique [17, 18], the time-of-flight absorption pictures and the corresponding visibility of ultracold Bose gases in a triangular optical lattice have been calculated analytically [16]. The comparison between our analytical results and the experimental data [19] exhibits a qualitative agreement. It should be emphasized that the practical advantage of re-summing technique is that it takes infinite high-order hopping into account in a systematic way so that it can be used to reveal the quantum properties of the systems in both insulating and compressible phases in the vicinity of the quantum phase boundaries, including the excitation spectra [20] and the time-of-flight absorption pictures [16].

However, the aforementioned hopping parameter perturbation approaches treat all lattice sites equally. So far they can only be used to cope with systems in homogeneous lattices. Moreover, since the Fourier transformation technique is involved, the Green's function method is difficult to use even for homogeneous systems in non-Bravais lattices like hexagonal lattices. More importantly, along with the progress of experimental methods and the deepening of theoretical studies, more and more efforts have been devoted to more complex systems, including systems with long-range interactions [21–25], multi-component [26, 27], frustrations [28–30], and superlattice structures [31–35]. These systems, in practice, should be treated as systems in inhomogeneous lattices, i.e., lattices consisting of multi-sublattices. Hence, it becomes important and urgent to generalize these powerful analytical methods in order to make them applicable for investigating the corresponding problems in inhomogeneous systems.

Recently, by taking Bose systems in square and cubic superlattices as examples, Wang *et al.* [36] have developed a generalized effective potential field theory which can be used to compute the quantum phase diagrams for multi-component Bose systems. In this paper, based on the perturbation philosophy, we are going to approach bipartite sublattice problems along an route via the method of Green's function. As is known [16], the Green's function can directly decrypt the information of the time-of-flight absorption picture and the visibility of Bose gases in an optical lattice. Meanwhile, for second order phase transitions, the divergence of Green's function may also be used to locate the phase boundaries [13, 18, 37]. In order to illustrate the generalized Green's function method, in the present paper, we deal with scalar Bose gases in two types of bipartite lattices, where the bipartite sublattice is caused by lattice structure like hexagonal lattice or caused by interaction such as a d-dimensional hypercubic lattice with nearest-neighbor interaction.

In hexagonal lattice, the zero and finite temperature phase diagrams are calculated analytically and the zero temperature phase diagrams are in good agreement with the first-order results obtained by effective potential method [10]. Furthermore, in hexagonal lattice, time-of-flight pictures are calculated analytically for the first time and these pictures are in accord with the experiment qualitatively [38]. In d-dimensional hypercubic lattice, we have calculated the phase diagrams with $zV = 0.4U$ and $zV = 1.1U$, where V is the nearest-neighbor interaction (more detail see Section 5). The results are the same with the mean field results when $d \to \infty$ [39, 40]. For finite d systems, these results coincide with Gutzwiller calculation. In square lattice ($d = 2$ hypercubic lattice), at $zV = 0.4U$, time-of-flight pictures are calculated analytically with the case of charge-density-wave(2,1)(CDW(2,1)) and MI(2,2) crossing the phase boundaries respectively. It is the evidence of the existence of a supersolid (SS) phase that peaks at $(\pm\frac{\pi}{a}, \pm\frac{\pi}{a})$ emerge in time-of-flight pictures when the system enters the compressible phase from CDW(2,1) phase.

The remainder of the paper is organized as follows: in order to make the paper more self-contained, we would like first to give a brief review of the cumulants expansion and re-summed methods of Green's function in Section 2. In Section 3, the effort is mainly concentrated on generalizing the Green's function method for multi-

sublattice ultracold Bose systems. With the help of the extended Green's function technique, we respectively calculate the phase boundaries of the incompressible localized ground states and the time-of-flight absorption pictures of an ultracold Bose system in two types of bipartite lattices. One is hexagonal lattice (Section 4) and the other is a hypercubic optical lattice with nearest-neighbor interaction (Section 5). Discussion is given in Section 6.

2 A brief review of the cumulants expansion and re-summed Green's function method

Scalar Bose gases trapped in a homogeneous optical lattice is depicted by the Bose–Hubbard Hamiltonian in Eq. (1), and the corresponding one particle Green's function $G(\tau', j' \mid \tau, j)$ of this system is defined as

$$G(\tau', j' \mid \tau, j) = \langle \hat{T}_\tau[\hat{a}^\dagger_{j'}(\tau')\hat{a}_j(\tau)]\rangle. \tag{3}$$

Here τ is the imaginary time, $\hat{T}_\tau$ is the imaginary time ordering operator, and $\langle\cdot\rangle$ denotes the average with respect to the full Hamiltonian in Eq. (1).

In fact, the information of the momentum space distribution function $n(\boldsymbol{k})$ of the system, which can be revealed by experiments directly via time-of-flight technique [14], is encrypted in the one particle Green's function. The momentum space distribution function reads

$$n(\boldsymbol{k}) = N_S \mid w(\boldsymbol{k}) \mid^2 \langle \hat{a}^\dagger_{\boldsymbol{k}}\hat{a}_{\boldsymbol{k}}\rangle, \tag{4}$$

where $\hat{a}^\dagger_{\boldsymbol{k}}$ and $\hat{a}_{\boldsymbol{k}}$ are the Fourier transformation of the operators in Eq. (1), i.e.,

$$\begin{aligned}\hat{a}^\dagger_i &= \frac{1}{\sqrt{N_S}}\sum_{\boldsymbol{k}_1}\hat{a}^\dagger_{\boldsymbol{k}_1}\mathrm{e}^{-\mathrm{i}\boldsymbol{k}_1\cdot\mathbf{r}_i},\\ \hat{a}_j &= \frac{1}{\sqrt{N_S}}\sum_{\boldsymbol{k}_2}\hat{a}_{\boldsymbol{k}_2}\mathrm{e}^{\mathrm{i}\boldsymbol{k}_2\cdot\mathbf{r}_j},\end{aligned} \tag{5}$$

with N_S being the total number of the lattice sites and $w(\boldsymbol{k})$ being the corresponding Wannier function in momentum space. It is observed that $\langle \hat{a}^\dagger_{\boldsymbol{k}}\hat{a}_{\boldsymbol{k}}\rangle = \lim_{\tau\downarrow 0} G(\tau \mid 0, \boldsymbol{k})$, while $G(\tau \mid 0, \boldsymbol{k}) = \langle \hat{T}_\tau[\hat{a}^\dagger(\tau)_{\boldsymbol{k}}\hat{a}(0)_{\boldsymbol{k}}]\rangle$ is exactly the one particle Green's function in the momentum space which is the Fourier transformation of $G(\tau', j' \mid \tau, j)$. Moreover, according to Laudau's theory of phase transitions [12, 13], for second order phase transitions, which is the case for SF-MI phase transition, the divergence of Green's function reveals the location of phase boundaries. Hence, it is necessary to calculate the one particle Green's function explicitly.

However, due to the non-commutativity of the hopping part $\hat{H}_1$ and the local part $\hat{H}_0$ of the Hamiltonian (1), the Green's function may be calculated perturbatively via the Dirac representation by treating the hopping term in the Hamiltonian (1) as the perturbation part [16–18], but for the opposite limit this will not lead to a SF-MI phase transition at all [41]. In Dirac picture, the one particle Green's function reads

$$G(\tau', j' \mid \tau, j) = \frac{\mathrm{Tr}\{\mathrm{e}^{-\beta\hat{H}_0}\hat{T}_\tau[\hat{a}^\dagger_{j'}(\tau')\hat{a}_j(\tau)\hat{u}(\beta,0)]\}}{\mathrm{Tr}\{\mathrm{e}^{-\beta\hat{H}_0}\hat{u}(\beta,0)\}}, \tag{6}$$

where $\hat{O}(\tau) = \mathrm{e}^{\tau\hat{H}_0}\hat{O}\mathrm{e}^{-\tau\hat{H}_0}$, and $\hat{u}(\beta,0) = \hat{T}_\tau\left[\exp\left(\int_0^\beta \mathrm{d}\tau\sum_{\langle i,j\rangle} J\hat{a}^\dagger_i(\tau)\hat{a}_j(\tau)\right)\right]$ is the evolution operator (setting $\hbar = 1$) [43].

The perturbative expansion of $\hat{u}(\beta,0)$ leads to terms like

$$\begin{aligned}&\frac{1}{n!}\sum_{i_1,j_1,\cdots,i_n,j_n} J_{i_1,j_1}\cdots J_{i_n,j_n}\int_0^\beta \mathrm{d}\tau_1\cdots\int_0^\beta \mathrm{d}\tau_n\\ &\times\langle\hat{T}_\tau[\hat{a}^\dagger_{j'}(\tau')\hat{a}_j(\tau)\hat{a}^\dagger_{i_1}(\tau_1)\hat{a}_{j_1}(\tau_1)\cdots\hat{a}^\dagger_{i_n}(\tau_n)\hat{a}_{j_n}(\tau_n)]\rangle_0\end{aligned} \tag{7}$$

in the expanded expression of $G(\tau', j' \mid \tau, j)$, where $\langle\hat{O}\rangle_0$ denotes an average quantity with respect to the unperturbed part $\hat{H}_0$ of the Hamiltonian and J_{ij} reads

$$J_{ij} = \begin{cases} J, & \text{if } i,\ j \text{ are nearest-neighbors of each other,}\\ 0, & \text{otherwise.}\end{cases} \tag{8}$$

Then the problem of calculating one particle Green's function $G(\tau', j' \mid \tau, j)$ is transformed to a problem of calculating the n-particle Green's function with respect to $\hat{H}_0$

$$\begin{aligned}&G^{(0)}_n(\tau'_1, i'_1; \cdots; \tau'_n, i'_n \mid \tau_1, i_1; \cdots; \tau_n, i_n)\\ &= \langle\hat{T}_\tau[\hat{a}^\dagger_{i'_1}(\tau'_1)\hat{a}_{i_1}(\tau_1)\cdots\hat{a}^\dagger_{i'_n}(\tau'_n)\hat{a}_{i_n}(\tau_n)]\rangle_0.\end{aligned} \tag{9}$$

However, the Wick's theorem becomes invalid due to the locality of the non-perturbed part of the Hamiltonian (1). Instead, we use the theory of linked-cluster expansion [16–18] to expand the n-particle Green's function in terms of the cumulants

$$\begin{aligned}&C^{(0)}_m(\tau'_1, \cdots, \tau'_m \mid \tau_1, \cdots, \tau_m)\\ &= \langle\hat{T}_\tau[\hat{a}^\dagger(\tau'_1)\hat{a}(\tau_1)\cdots\hat{a}^\dagger(\tau'_m)\hat{a}(\tau_m)]\rangle_0\end{aligned} \tag{10}$$

in which the particle operators are all at the same site. Each annihilation operator in $G^{(0)}_n(\tau'_1, i'_1; \cdots; \tau'_n, i'_n \mid \tau_1, i_1; \cdots; \tau_n, i_n)$ must be paired by a creation operator at the same site due to the locality of the eigenstates of $\hat{H}_0$.

The decomposition of the above mentioned n-particle Green's function in terms of these cumulants is quite straightforward. For instance, the decompositions of one and two particle Green's functions are shown in the fol-

lowing

$$G_1^{(0)}(\tau', i' \mid \tau, i) = \delta_{i',i}\, C_1^{(0)}(\tau' \mid \tau), \tag{11}$$

$$\begin{aligned} &G_2^{(0)}(\tau_1', i_1'; \tau_2', i_2' \mid \tau_1, i_1; \tau_2, i_2) \\ &= \delta_{i_1',i_1}\delta_{i_1',i_2'}\delta_{i_1,i_2}\, C_2^{(0)}(\tau_1', \tau_2' \mid \tau_1, \tau_2) \\ &\quad + \delta_{i_1',i_1}\delta_{i_2',i_2} C_1^{(0)}(\tau_1' \mid \tau_1) C_1^{(0)}(\tau_2' \mid \tau_2) \\ &\quad + \delta_{i_1',i_2}\delta_{i_2',i_1} C_1^{(0)}(\tau_1' \mid \tau_2) C_1^{(0)}(\tau_2' \mid \tau_1). \end{aligned} \tag{12}$$

All these expressions can be diagrammatized as

$C_1^{(0)}(\tau' \mid \tau) =$ 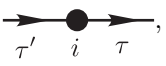

, (13)

$C_2^{(0)}(\tau_1', \tau_2' \mid \tau_1, \tau_2) =$ 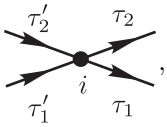

, (14)

where the pointing-in arrows represent creation operators and the pointing-out arrows represent annihilation operators. The hopping parameter J_{ij} may be represented correspondingly as

$J_{ij} =$ 

. (15)

When considering the cancellation effect of the numerator and the denominator in Eq. (6), the one particle Green's function $G(\tau', j' \mid \tau, j)$ only consists of connected diagrams.

Perturbative calculation of Green's function needs us to re-group all the connected diagrams based on the properties of loops in diagrams instead of the order of J/U, since finite-order perturbative calculation always presents a polynomial and cannot reflect the divergence of Green's function at phase transition point. This is the so-called re-summed Green's function technique [18, 37, 42]. In fact, the re-summed hopping expansion can also be looked upon as a $1/d$ expansion of a d-dimensional system, thus can be used to properly describe the quantum critical behaviour of the lattice quantum gas.

3 The generalized Green's function method

For interested cases, normal Bose–Hubbard model in hexagonal lattice and extended Bose Hubbard model (EBHM) in d-dimensional hypercubic lattice, we can easily know the ground-state configurations of $\hat{H}_0$ (See Section 5 for EBHM). Switching on the hopping parameter J gradually, the localized ground states will be softened by the quantum fluctuations and will transform into some delocalized and compressible phases (either SF or SS phase) when J goes beyond some critical value. These phase transitions are entirely caused by the quantum fluctuations due to the noncommutativity of the local and hopping parts in the full Hamiltonian, and therefore are the so-called quantum phase transitions [4]. As is confirmed [3, 44], these quantum phase transitions are second-order phase transitions. The actual phase boundaries of the localized phases need to be determined quantitatively in an analytical way and we are going to tackle this problem along the avenue of Green's function. This also provides us an opportunity to illustrate the generalized re-summed Green's function method clearly.

As is known [16–18], the Green's function method reviewed in the preceding section is for homogeneous lattice structures, hence needs to be generalized in order to treat the present problem.

We again look upon the hopping parameter as perturbation, i.e., that the unperturbed states are the localized phases is obvious in hexagonal lattice systems and will be discussed in d-dimensional hypercubic lattice systems. Formally, the one-particle Green's function $G^{\mathrm{inh}}(\tau', j'|\tau, j)$ for the bipartite lattice takes the same form as in Eq. (6) for the case of homogeneous lattice, but with an extra term of nearest-neighbor repulsive interaction in $\hat{H}_0$ expressed in Eq. (41) (for EBHM). In the same manner, the evolution operator $\hat{u}(\beta, 0)$ in the numerator and denominator should also be expanded perturbatively with respect to the hopping amplitude J, hence this again transforms the problem of calculating the one-particle Green's function $G^{\mathrm{inh}}(\tau', j'|\tau, j)$ to the problem of calculating n-particle Green's functions $G_n^{(0)}(\tau_1', i_1'; \cdots; \tau_n', i_n' \mid \tau_1, i_1; \cdots; \tau_n, i_n) = \langle \hat{T}_\tau[\hat{a}_{i_1'}^\dagger(\tau_1')\hat{a}_{i_1}(\tau_1)\cdots; \hat{a}_{i_n'}^\dagger(\tau_n')\hat{a}_{i_n}(\tau_n)]\rangle_0$ with respect to $\hat{H}_0$. Due to the locality of the states determined by $\hat{H}_0$, $G_n^{(0)}(\tau_1', i_1'; \cdots; \tau_n', i_n' \mid \tau_1, i_1; \cdots; \tau_n, i_n)$ may be calculated analytically via cumulants expansion technique.

Generally, sublattices A and B of bipartite lattice are distinguishable and the local properties of lattice sites belonging to different sublattices are different. Hence, in calculating the n-particle Green's functions $G_n^{(0)}(\tau_1', i_1'; \cdots; \tau_n', i_n' \mid \tau_1, i_1; \cdots; \tau_n, i_n)$, cumulants on different sublattices need to be discriminated. In bipartite lattices systems, there are two different groups of cumulants

$$C_{nA}^{(0)} = \langle \hat{T}_\tau[\hat{a}_A^\dagger(\tau_1')\hat{a}_A(\tau_1)\cdots\hat{a}_A^\dagger(\tau')\hat{a}_A(\tau)]\rangle_0 \tag{16}$$

and

$$C_{nB}^{(0)} = \langle \hat{T}_\tau[\hat{a}_B^\dagger(\tau_1')\hat{a}_B(\tau_1)\cdots\hat{a}_B^\dagger(\tau')\hat{a}_B(\tau)]\rangle_0, \tag{17}$$

in which a_A ($a_A^\dagger$) and a_B ($a_B^\dagger$) are operators on sublattices A and B, respectively. The cumulants may be

diagrammatized, for instance, as follows:

$$C^{(0)}_{1A}(\tau' \mid \tau) =$$ 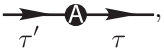

$$C^{(0)}_{1B}(\tau' \mid \tau) =$$ 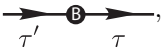

(18)

$$C^{(0)}_{2A}(\tau'_1, \tau'_2 \mid \tau_1, \tau_2) =$$ 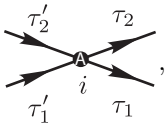

$$C^{(0)}_{2B}(\tau'_1, \tau'_2 \mid \tau_1, \tau_2) =$$ 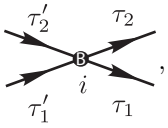

(19)

where the pointing-in arrows represent creation operators and the pointing-out arrows represent annihilation operators.

In principle, the one-particle Green's function for the inhomogeneous lattice Bose systems may be calculated accurately by counting contribution of all connected diagrams consisting of all nonvanishing cumulants and hoppings. Formally, it can be expressed diagrammatically as

$$G^{\mathrm{inh}}(\tau', i|\tau, j) =$$ 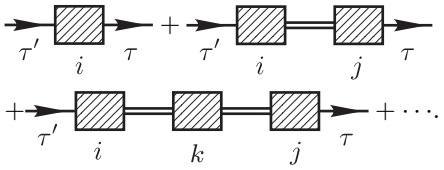

(20)

The squares in the diagrams represent the contribution from all non-vanishing cumulants together with hoppings, double-lines represent all possible hopping connections between nearest-neighbor sites, and these diagrams may include loops.

In practice, one needs to calculate the Green's function perturbatively by selecting a specific group of diagrams in a proper way. As is well known [12, 13], Green's functions should be diverging in the vicinity of second-order phase transition point. However, this property cannot be exposed just by counting finite orders of the perturbation parameter J/U, since a polynomial will always be finite. Hence, we re-group the diagrams based on the properties of loops in each diagram rather than the order of J/U, and then each group now consists of infinite number of diagrams. This is the so-called re-summed Green's function technique [16, 18, 37]. At present, for simplicity, we only consider the resummed Green's function $\tilde{G}^{\mathrm{inh}}_1$ containing only diagrams of chains consisting of first order cumulants and hopping between sites. In terms of Matsubara frequency, the re-summed Green's function reads

$$\tilde{G}^{\mathrm{inh}}_1(\omega_m, i, j) =$$ 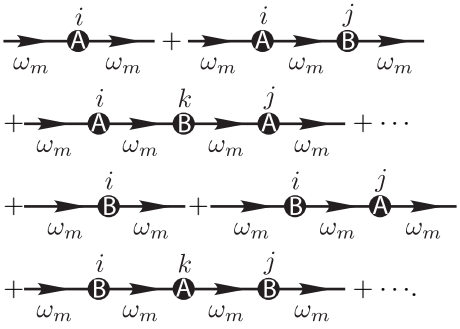

(21)

In fact, the present choice of the re-summed Green's function may be looked upon as a sort of mean field treatment [16, 18], and is going to be accurate when the dimension of the system d goes to infinity. However, from the discussion, it is clear to see that the re-summed Green's function method can in principle go beyond mean field by adding loop diagrams constituted by higher-order cumulants and related hoppings.

The above re-summed Green's function diagrams can be re-expressed mathematically in terms of first-order cumulants and hopping parameters in momentum-space as

$$\begin{aligned}\tilde{G}^{\mathrm{inh}}_1(\omega_m, \boldsymbol{k}) = & C^{(0)}_{1A}(\omega_m) + C^{(0)}_{1A}(\omega_m) C^{(0)}_{1B}(\omega_m) J_{AB}(\boldsymbol{k}) \\ & + [C^{(0)}_{1A}(\omega_m)]^2 C^{(0)}_{1B}(\omega_m) J_{AB}(\boldsymbol{k}) J_{BA}(\boldsymbol{k}) + \cdots \\ & + C^{(0)}_{1B}(\omega_m) + C^{(0)}_{1B}(\omega_m) C^{(0)}_{1A}(\omega_m) J_{BA}(\boldsymbol{k}) \\ & + [C^{(0)}_{1B}(\omega_m)]^2 C^{(0)}_{1A}(\omega_m) J_{BA}(\boldsymbol{k}) J_{AB}(\boldsymbol{k}) + \cdots\end{aligned} \tag{22}$$

where the cumulant in Matsubara frequency and hopping in momentum-space read

$$C^{(0)}_{1A(B)}(\omega_m) = \int_0^\beta C^{(0)}_{1A(B)}(\tau) \mathrm{e}^{\mathrm{i}\omega_m \tau} \mathrm{d}\tau \tag{23}$$

and

$$J_{AB/BA}(\boldsymbol{k}) = \sum_{ij} J_{ij} \mathrm{e}^{\mathrm{i}\boldsymbol{k}\cdot\boldsymbol{r}_i} \mathrm{e}^{-\mathrm{i}\boldsymbol{k}\cdot\boldsymbol{r}_j} \quad (i \in A/B), \tag{24}$$

respectively. Since $C^{(0)}_1(\tau) = \langle \hat{T}_\tau[\hat{a}^\dagger(\tau)\hat{a}(0)]\rangle_0$, by counting the detailed information of the eigenstates of $\hat{H}_0$, a complicated yet straightforward calculation leads to

$$\begin{aligned}C^{(0)}_{1A}(\omega_m) = \frac{1}{Z^{(0)}} \sum_{n_A, n_B=0}^{\infty} \Bigg[& \frac{n_A + 1}{E_{n_A+1, n_B} - E_{n_A, n_B} + \mathrm{i}\omega_m} \\ & - \frac{n_A}{E_{n_A, n_B} - E_{n_A-1, n_B} + \mathrm{i}\omega_m} \Bigg] \mathrm{e}^{-\beta E_{n_A, n_B}},\end{aligned} \tag{25}$$

and

$$C_{1B}^{(0)}(\omega_m)=\frac{1}{Z^{(0)}}\sum_{n_A,n_B=0}^{\infty}\left[\frac{n_B+1}{E_{n_A,n_B+1}-E_{n_A,n_B}+\mathrm{i}\omega_m}-\frac{n_B}{E_{n_A,n_B}-E_{n_A,n_B-1}+\mathrm{i}\omega_m}\right]\mathrm{e}^{-\beta E_{n_A,n_B}},\tag{26}$$

where $Z^{(0)}=\sum_{n_A,n_B=0}^{\infty}\mathrm{e}^{-\beta E_{n_A,n_B}}$. So far we have presented the generalized Green's function in momentum space for bipartite lattices. It will be used to study the phase diagrams and time-of-flight absorption pictures in two types of bipartite optical lattices in the next two sections.

4 Phase diagrams and time-of-flight pictures of scalar Bose atoms in hexagonal optical lattice

Recently, multi-component quantum Bose gases in spin-dependent hexagonal lattices have been realized in the experiment [38]. The time-of-flight absorption pictures for different polarization states have been observed in the experiment. So far, only a numerical Gutzwiller approach have been used to obtain time-of-flight absorption pictures in theory for hexagonal lattice systems. Here, we will introduce a new method: the generalized Green's function method, which can be used to obtain the phase diagrams and the time-of-flight absorption pictures for ultracold Bose gases in hexagonal optical lattice analytically. In hexagonal optical lattice, the time-of-flight absorption pictures obtained by generalized Green's function method are in accord with the experiment qualitatively. It is the first time that time-of-flight absorption pictures is obtained by analytical method in hexagonal lattice.

In the experiment [38], the $F=1$ hyperfine ground-states of ^{87}Rb in spin-dependent hexagonal lattices has been realized. Here, we are only interested in $|1,0\rangle$ state that is one of $F=1$ hyperfine ground-states. Since $m_f=0$, the trapping potential of $|1,0\rangle$ state is independent on the sublattice sites [38]. In that case, filling factors of the different sublattices of the hexagonal lattice are equal. It leads to $C_{1A}^{(0)}=C_{1B}^{(0)}$, then the resummed Green's function can be reduced as

$$\begin{aligned}G^{inh}(\omega_m,\boldsymbol{k})=&\sum_{l=0}^{\infty}[C_{1A}^{(0)}(\omega_m)]^{2+2l}[J_{AB}(\boldsymbol{k})+J_{BA}(\boldsymbol{k})][J_{AB}(\boldsymbol{k})J_{BA}(\boldsymbol{k})]^l\\&+\sum_{l=0}^{\infty}2[C_{1A}^{(0)}(\omega_m)]^{2l+1}[J_{AB}(\boldsymbol{k})J_{BA}(\boldsymbol{k})]^l.\end{aligned}\tag{27}$$

If the relation

$$1-C_{1A}^{(0)}(\omega_m)C_{1A}^{(0)}(\omega_m)[J_{AB}(\boldsymbol{k})J_{BA}(\boldsymbol{k})]=0\tag{28}$$

is satisfied, the Green's function will be divergent, where the hopping term $J_{AB}(\boldsymbol{k})=J\left[\mathrm{e}^{\mathrm{i}k_xa}+2\mathrm{e}^{-\mathrm{i}k_x\frac{a}{2}}\cos\left(\frac{\sqrt{3}ak_y}{2}\right)\right]$ represents Fourier transformation of the hopping process from A sublattice to B sublattice and the hopping term $J_{BA}(\boldsymbol{k})=J\left[\mathrm{e}^{-\mathrm{i}k_xa}+2\mathrm{e}^{\mathrm{i}k_x\frac{a}{2}}\cos\left(\frac{\sqrt{3}ak_y}{2}\right)\right]$ denotes the opposite process. By taking into account that the phase transitions occur due to long-wavelength fluctuations [12, 13], the above formula determines the locations of the phase boundaries of localized states via the equation below

$$zJ_c=\frac{1}{C_{1A}^{(0)}(\omega_m=0)}.\tag{29}$$

At zero temperature, the eigenstates of the unperturbed part $\hat{H}_0$ fall into the ground states. From the experiment [38], since filling factors of the different sublattice of the hexagonal lattice are equal($n_A=n_B=n$), the phase-boundary equation Eq. (29) is then reduced to

$$zJ_c=\frac{1}{\frac{n+1}{E_{n+1,n}-E_{n,n}}-\frac{n}{E_{n,n}-E_{n-1,n}}}.\tag{30}$$

Using Eqs. (29) and (30), we can obtain not only the zero temperature but also finite temperature phase diagrams which are presented in Fig. 1. The zero temperature phase diagrams obtained by generalized Green's function method are the same as first-order (mean-field) results got by effective potential method [10], but effective potential method can not be used to obtain the finite temperature phase diagrams.

Unfortunately, the phase boundaries calculated above are not quantities which can directly reveal the features of both insulating and compressible phases in experiment. Instead, one of these quantities is the momentum distribution function probed by time-of-flight measurement [3], which represents the standard experimental technique for investigating cold atomic systems in optical lattices [1, 45, 46]. The advance of the generalized Green's function method is not only to obtain finite or zero temperature phase diagrams but also to get the time-of-flight absorption pictures for ultracold scalar Bose systems. In this section, with the help of the generalized Green's function developed in the preceding section, we will calculate the time-of-flight pictures of an ultraclod scalar Bose gases with Bose–Hubbard interaction in a hexagonal optical lattice.

In principle, it is impossible to create a real 2D optical lattice ultracold particle system experimentally, but in practice, the 2D character can be achieved by setting

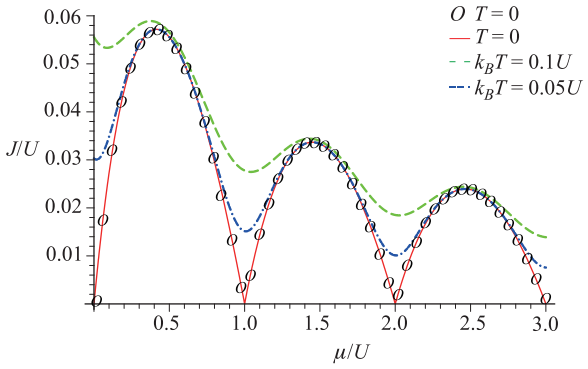

Fig. 1 The quantum phase diagrams of a Bose system in a hexagonal lattice with zero temperature and finite temperature. The red solid lines, the green dashed lines and the blue dashed lines, which are obtained by the generalized Green's function method, denote location of phase boundaries of the zero temperature, $k_BT = 0.1U$ and $k_BT = 0.05U$ respectively. The empty circles denote the first-order zero temperature phase boundaries obtain by effective potential method [10], and coincide with the red solid line.

the optical lattice depth in the third space dimension to a sufficient high value in order to restrict the hopping of particles between layers [46–48].

Before to calculate the time-of-flight pictures, we need to know the explicit form of J and U with the trapping potential. The hexagonal optical lattice has been realized in the experiment [38] and the trapping potential of $|1,0\rangle$ state is described mathematically by

$$V(\boldsymbol{r}) = -2V_0\left[3-\cos\left(-\frac{\sqrt{3}\pi x}{\lambda}+\frac{3\pi y}{\lambda}\right)+\cos\left(\frac{\sqrt{3}\pi x}{\lambda}+\frac{3\pi y}{\lambda}\right)+\cos\left(\frac{2\sqrt{3}\pi x}{\lambda}\right)\right], \tag{31}$$

where $\lambda = 830$ nm is the wavelength of the lattice laser beams which are used to create hexagonal optical lattice. The lattice constant of the hexagonal optical lattice is $a = \frac{2\lambda}{3\sqrt{3}}$. Using the harmonic approximation at the minimum trapping potential point, the trapping potential is separable, thus the 2D Wannier function $w(\boldsymbol{r}-\boldsymbol{r}_i)$ in the xy-plane is given as

$$w(\boldsymbol{r}-\boldsymbol{r}_i) = \left(\frac{64\widetilde{V}_0}{81}\right)^{\frac{1}{4}}\left(\frac{\pi}{a^2}\right)^{\frac{1}{2}}\exp\left[-\sqrt{\frac{16\widetilde{V}_0}{81}}\times\frac{\pi^2}{a^2}\left[(x-x_i)^2+(y-y_i)^2\right]\right], \tag{32}$$

where $\widetilde{V}_0$ is the dimensionless optical lattice depth in units of E_R and $E_R = (\hbar^2k^2)/2m$ ($k = 2\pi/\lambda$) is the recoil energy. The forms of J and U reads [6]

$$J = -\int \mathrm{d}\boldsymbol{r} w^*(\boldsymbol{r}-\boldsymbol{r}_i)\left(-\frac{\hbar^2\nabla^2}{2m}+V(\boldsymbol{r})\right)w(\boldsymbol{r}-\boldsymbol{r}_j) \tag{33}$$

and

$$U = g\int \mathrm{d}\boldsymbol{r}|w(\boldsymbol{r})|^4 \tag{34}$$

respectively, where $w(\boldsymbol{r}-\boldsymbol{r}_j)$ is the Wannier functions and $\boldsymbol{r}_i$, $\boldsymbol{r}_j$ denote the nearest neighboring sites. Inserting Eq. (32) into the Eq. (33), J takes the from

$$J = E_R\left(\frac{\pi^2}{3}+8-\frac{5}{2\sqrt{\widetilde{V}_0}}\right)\widetilde{V}_0\mathrm{e}^{-\frac{2\pi^2\sqrt{\widetilde{V}_0}}{9}}. \tag{35}$$

Because in the third direction(z direction) the lattice is a simple square lattice, then the lattice length reads $b = \frac{\lambda}{2} = \frac{3\sqrt{3}a}{4}$ in the third dimension. In z dimension, the Wannier function takes form

$$w(z-z_i) = (44)^{\frac{1}{8}}\left(\frac{\pi}{b^2}\right)^{\frac{1}{4}}\exp\left[-\frac{\pi^2}{2}\sqrt{44}\frac{(z-z_i)^2}{b^2}\right], \tag{36}$$

where the 44 (take the units of recoil energies E_R) is the trapping potential [38]. Now we can obtain U as

$$U = \frac{4\sqrt{6}}{3}E_R\frac{a_s}{a}(\pi\widetilde{V}_0)^{1/2}(44)^{1/4}, \tag{37}$$

by inserting Eqs. (32) and (36) into Eq. (34).

Thus, the momentum distribution function of an optical lattice ultracold Bose system reads

$$n(\boldsymbol{k}) = N_S \mid w(\boldsymbol{k}) \mid^2 \lim_{\tau\downarrow 0} G(\tau \mid 0,\boldsymbol{k}), \tag{38}$$

where $w(\boldsymbol{k})$ is the Fourier transformation of $w(\boldsymbol{r})$ and $G(\tau \mid 0,\boldsymbol{k}) = \langle\hat{T}_\tau[\hat{a}^\dagger_{\boldsymbol{k}}\hat{a}_{\boldsymbol{k}}]\rangle$ is the one-particle Green's function in the momentum space. At $T = 0$, we get, to the lowest order, the one-particle Green's function in terms of Matsubara frequency given in Eq. (27), which in turn leads to

$$G(\tau|0,\boldsymbol{k}) = \frac{1}{2\pi}\int_{-\infty}^{+\infty}\mathrm{d}\omega_m G^{\mathrm{inh}}(\omega_m,\boldsymbol{k})\mathrm{e}^{-\mathrm{i}\omega_m\tau}. \tag{39}$$

Together with Eqs. (25) and (26), the momentum distribution function in Eq. (38) can in principle be calculated out analytically. In the experiment, we know that the filling factor is $n = 1$ and the $a_s = 5.34$ nm is the s-wave scattering length of the ^{87}Rb. Using Eqs. (35), (37) and (38), we can plot time-of-flight absorption pictures in Fig. 2, which are pictures of the momentum distribution $n(\boldsymbol{k})$ as function of the lattice depth $\widetilde{V}_0$. The time-of-flight absorption pictures clearly show that the SF-MI

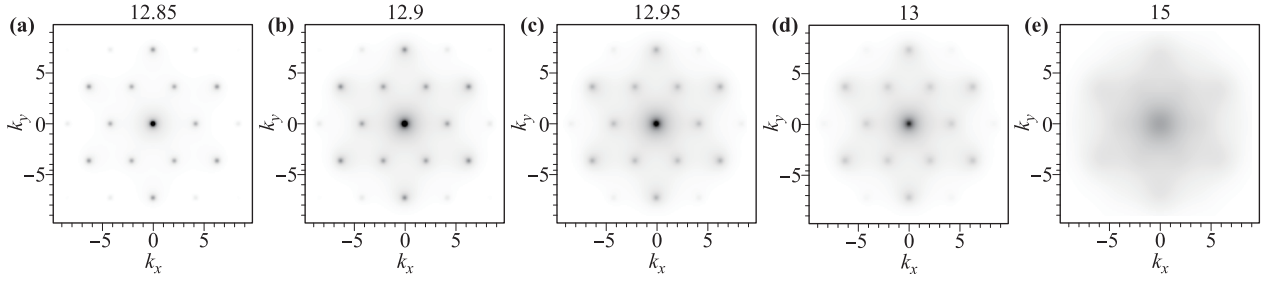

Fig. 2 Time-of-flight absorption pictures for ultracold scalar Bose systems in hexagonal lattice at zero temperature. k_x and k_y in the plots take the units of $\frac{1}{a}$. The MI-SF quantum phase transition is shown from TOF picture, and the critical point is about in the region $12.85 \leq \widetilde{V}_0 \leq 13$.

phase transition appear in the region $12.85 \leq \widetilde{V}_0 \leq 13$ and this result is consistent with the critical trapping potential $\widetilde{V}_0 = 12.947$ which is obtained from Fig. 1 together with Eqs. (35) and (37). This result is also in accord with the Gutzwiller calculation which shows that the superfluid order parameter will be zero near the point of $\widetilde{V}_0 = 13$ [38]. Moreover, in principe, this generalized Green's function method can also be used to deal with case of $|1, m_f \neq 0\rangle$ state in the spin-dependent hexagonal lattice.

5 Phase diagrams and time-of-flight pictures of Bose gases with nearest neighbour repulsive interaction in d-dimensional hypercubic lattice

In the previous section, we study phase diagrams and time-of-flight pictures of scalar Bose atoms in the hexagonal optical lattice, where the bipartite systems are caused by lattice structure. In this section, we concentrate on systems of ultracold bosons with nearest-neighbor repulsion in d-dimensional hypercubic optical lattices. These systems are described by the EBHM

$$\hat{H}_{\mathrm{EBHM}} = \hat{H}_1 + \hat{H}_0, \tag{40}$$

where

$$\hat{H}_0 = \sum_i \left[\frac{U}{2}\hat{n}_i(\hat{n}_i - 1) - \mu\hat{n}_i\right] + V\sum_{\langle i,j\rangle}\hat{n}_i\hat{n}_j,$$
$$\hat{H}_1 = -J\sum_{\langle i,j\rangle}\hat{a}_i^\dagger\hat{a}_j. \tag{41}$$

Now, the local part $\hat{H}_0$ includes the nearest-neighbor repulsive interaction V. Due to this nearest-neighbor interaction, the hypercubic lattice is naturally divided into two sublattices, i.e., it has bipartite lattice structure, as sketched in Fig. 3.

The subtle balance between the hopping parameter J, onsite repulsion U and nearest-neighbor repulsion V introduces rich phase structures to this system. Similarly, we treat the hopping parameter J as a perturbation. However, even if J takes the value of 0, the competition between U and V will lead to different localized phases at zero temperature. In order to calculate the phase boundaries of the localized phases, the localized phases at $J = 0$ need to be clarified first. This can be achieved easily by the following analysis.

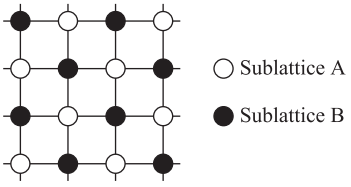

Fig. 3 Sketch of the sublattice structure of the nearest-neighbor interacting Bose system in square lattice.

Let us play a game of throwing bosons into the lattice. Suppose the total number of lattice sites is N. Due to the nearest-neighbor repulsion, the first $\frac{N}{2}$ particles will fill up either sublattice A or sublattice B, let us say, sublattice A. Where the next $\frac{N}{2}$ bosons go is determined by the relative strength of U and zV (z is the number of nearest-neighbor sites, in present case $z = 2d$).

Suppose $U > zV$, for the reason of energy, the second group of $\frac{N}{2}$ bosons will fill up the sublattice B. Without loss of generality, let the filling factor n_A of sublattice A be always larger than or equal to n_B of sublattice B. Apparently, in this case, the third group will go to sublattice A, then followed by filling up sublattice B, and so forth. In other words, $n_A - n_B$ is either 1 or 0. We denote these localized states by $|n_A, n_B\rangle$. Here, $|n, n\rangle$ is called MI states, and $|n+1, n\rangle$ is the so-called CDW states. All these localized states are eigenstates of $\hat{H}_0$ and the corresponding eigenergies read

$$\hat{H}_0\,|n_A, n_B\rangle = \frac{N}{2}E_{n_A,n_B}\,|n_A, n_B\rangle\,,$$
$$E_{n_A,n_B} = \frac{U}{2}n_A(n_A - 1) + \frac{U}{2}n_B(n_B - 1) + zVn_An_B - \mu(n_A + n_B). \tag{42}$$

The constraint on the chemical potential μ in each Mott region is determined by solving the equations $E_{n,n} \leq E_{n+1,n}$ and $E_{n,n} \leq E_{n,n-1}$. This leads to

$$U(n-1)+zVn \leq \mu \leq Un+zVn. \tag{43}$$

Similarly, we get for the CDW regions that

$$U(n-1)+zV(n-1) \leq \mu \leq U(n-1)+zVn. \tag{44}$$

For the case of $U < zV$, it is not difficult to figure out that bosons always go to sublattice A, i.e., $n_A = n$ while $n_B = 0$, the ground state is always CDW state $|n,0\rangle$, and the chemical potential for each filling factor n satisfies

$$U(n-1) \leq \mu \leq Un. \tag{45}$$

When $U = zV$, it is known [49] that the CDW state $(n+1,n)$ becomes degenerate with the CDW state $(2n+1,0)$, and the Mott state (n,n) becomes degenerate with the CDW state $(2n,0)$. This case will not be discussed in the present paper. From Eq. (22), it is recognized that divergence of the Green's function requires

$$1 - C_{1A}^{(0)}(\omega_m)C_{1B}^{(0)}(\omega_m)J^2(\boldsymbol{k}) = 0, \tag{46}$$

since $J_{AB}(\boldsymbol{k})$ is equal to $J_{BA}(\boldsymbol{k})$ in hypercubic lattices. As similar with the case of hexagonal lattice, in d-dimensional hypercubic lattice, the locations of phase boundaries of localized states satisfy the equation below

$$z^2J_c^2 = \frac{1}{C_{1A}^{(0)}(\omega_m=0)C_{1B}^{(0)}(\omega_m=0)}. \tag{47}$$

Moreover, at zero temperature, the phase-boundary equation Eq. (47) is then reduced to

$$z^2J_c^2 = \frac{1}{\frac{n_A+1}{E_{n_A+1,n_B}-E_{n_A,n_B}} - \frac{n_A}{E_{n_A,n_B}-E_{n_A-1,n_B}}} \times \frac{1}{\frac{n_B+1}{E_{n_A,n_B+1}-E_{n_A,n_B}} - \frac{n_B}{E_{n_A,n_B}-E_{n_A,n_B-1}}}, \tag{48}$$

where the filling factors of sublattices A and B in the ground state are n_A and n_B.

By substituting the eigenvalues in Eq. (42) into the above equation, we finally get the analytical expression of the quantum phase boundaries of the system

$$\frac{1}{z^2J_c^2} = \left[\frac{n_A+1}{Un_A+zVn_B-\mu} - \frac{n_A}{U(n_A-1)+zVn_B-\mu}\right] \times \left[\frac{n_B+1}{Un_B+zVn_A-\mu} - \frac{n_B}{U(n_B-1)+zVn_A-\mu}\right]. \tag{49}$$

As examples, we show the phase diagrams for the system with $zV = 0.4U$ and $zV = 1.1U$ in Figs. 4(a) and (b), respectively. Our analytical results from extended re-summed Green's function method become exactly the same as the mean field results when $d \to \infty$ [39, 40], consistent with preceding discussion. Moreover, for finite d systems, our analytical results obtained by extended re-summed Green's function method are consistent with the Gutziwiller calculation [49] (see Fig. 4), but via the divergence of Green's function, this Green's function method can not ascertain that this compressible phase is SS phase or SF phase. As shown in Section 4, the Green's function can reveal the quantum properties of the systems in both insulating and compressible phase

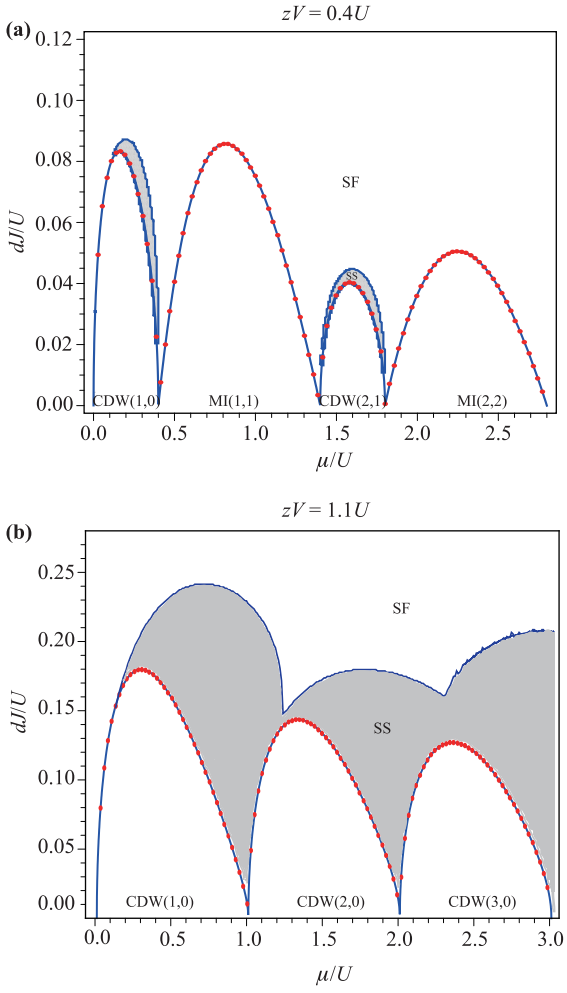

Fig. 4 The quantum phase diagrams of a Bose system in a d-dimensional hypercubic lattice with nearest-neighboring repulsive interaction V for cases of **(a)** $zV = 0.4U$ and **(b)** $zV = 1.1U$. The red dotted lines are obtained by Green's function method and the blue lines are obtained by Gutzwiller approach (for (b) blue lines date are from Ref. [49]). Obviously, the phase boundaries of localized phases (MI or CDW)-compressible phase (SS or MI) obtained by these two methods are exactly the same, but our Green's function method can not ascertain that this compressible phase is SS phase or SF phase.

in the vicinity of the phase boundaries by counting the time-of-flight absorption pictures. At the below, we will show how to identify SS phase and SF phase form the different features of their time-of-flight absorption pictures. While there is only peaks around $\boldsymbol{k}=(0,0)$ and reciprocal lattice vectors for the SF phase, an additional satellite peaks at $\boldsymbol{k}=(\pm\frac{\pi}{a},\pm\frac{\pi}{a})$ (for this paper) would give evidence to the SS phase [50].

As is known, the EBHM with nearest-neighbor interaction in Eq. (40) is the one-band approximation of the following many-body Hamiltonian under extreme low temperature limit [51]

$$H=\int \mathrm{d}\boldsymbol{r}\psi^{\dagger}(\boldsymbol{r})\left(-\frac{\hbar^2}{2m}\nabla^2+V(\boldsymbol{r})\right)\psi(\boldsymbol{r}) +\frac{1}{2}\iint \mathrm{d}\boldsymbol{r}_1\mathrm{d}\boldsymbol{r}_2\psi^{\dagger}(\boldsymbol{r}_1)\psi^{\dagger}(\boldsymbol{r}_2)V(\boldsymbol{r}_1-\boldsymbol{r}_2)\psi(\boldsymbol{r}_2)\psi(\boldsymbol{r}_1). \tag{50}$$

Here, $V(\boldsymbol{r})=V_0\sin^2(\pi x/a)+V_0\sin^2(\pi y/a)+V_3\sin^2(\pi z/a)$ is the optical lattice trapping potential (the lattice depth in z-direction V_3 is larger than the lattice depth V_0 in other two-direction due to the fact that we emphasized in previous section) and the two-particle interaction $V(\boldsymbol{r}_1-\boldsymbol{r}_2)$ consists of a contact term and a dipole-dipole part:

$$V(\boldsymbol{r}_1-\boldsymbol{r}_2)=g\delta(\boldsymbol{r}_1-\boldsymbol{r}_2)+\frac{C_{dd}}{4\pi}\frac{1-3\cos^2\theta}{|\boldsymbol{r}_1-\boldsymbol{r}_2|^3}, \tag{51}$$

where $g=4\pi\hbar^2a_s/m$ (a_s is the 3D s-wave scattering length of the Bose particles and m is the corresponding mass) is the contact interaction strength, C_{dd} is the coupling constant ($C_{dd}=m_e^2/\epsilon_0$ for the case of electric dipole moments m_e and $C_{dd}=m_m^2\mu_0$ for the case of magentic dipole moments m_m), and θ is the angle between the polarization direction of the two interacting dipoles. In this tight-binding limit, the dipolar term [52] in Eq. (50) gives

$$H_d=\frac{1}{2}\iint \mathrm{d}\boldsymbol{r}_1\mathrm{d}\boldsymbol{r}_2\hat{\psi}^{\dagger}(\boldsymbol{r}_1)\hat{\psi}^{\dagger}(\boldsymbol{r}_2)U_{dd}(\boldsymbol{r}_1-\boldsymbol{r}_2)\hat{\psi}(\boldsymbol{r}_2)\hat{\psi}(\boldsymbol{r}_1). \tag{52}$$

In the Wannier basis, we can get

$$H_d=\sum_{i,j,k,l}V_{i,j,k,l}\hat{a}_i^{\dagger}\hat{a}_j^{\dagger}\hat{a}_k\hat{a}_l, \tag{53}$$

where the matrix elements $V_{i,j,k,l}$ are given by the integral

$$V_{i,j,k,l}=\frac{1}{2}\iint \mathrm{d}\boldsymbol{r}_1\mathrm{d}\boldsymbol{r}_2w^*(\boldsymbol{r}_1-\boldsymbol{R}_i)\,w^*(\boldsymbol{r}_2-\boldsymbol{R}_j) \times U_{dd}(\boldsymbol{r}_1-\boldsymbol{r}_2)\,w(\boldsymbol{r}_1-\boldsymbol{R}_k)\,w(\boldsymbol{r}_2-\boldsymbol{R}_l). \tag{54}$$

For the deep enough optical potentials, we can assume σ (σ is the spatial localization length of the Wannier function) to be much smaller than the optical lattice spacing a. In this limit, the Wannier function $w(\boldsymbol{r}-\boldsymbol{R}_i)$ is significantly non-zero for $\boldsymbol{r}\approx\boldsymbol{R}_i$. Thus, non-zero $V_{i,j,i,j}$ appears only for $i=k$ and $j=l$, and then $V_{i,j,k,l}$ can be divided by the off-site part $V_{i,j,i,j}$ ($i\neq j$),

$$\begin{aligned}V_{i,j,i,j}&\approx U_{dd}(\boldsymbol{R}_i-\boldsymbol{R}_j)\frac{1}{2}\iint \mathrm{d}\boldsymbol{r}_1\mathrm{d}\boldsymbol{r}_2w^*(\boldsymbol{r}_1-\boldsymbol{R}_i) \times w^*(\boldsymbol{r}_2-\boldsymbol{R}_j)\,w(\boldsymbol{r}_1-\boldsymbol{R}_i)\,w(\boldsymbol{r}_2-\boldsymbol{R}_j)\\ &=\frac{C_{dd}\left(1-3\cos^2\theta\right)}{8\pi a^3}=V,\end{aligned} \tag{55}$$

and the on-site part $V_{i,i,i,i}$,

$$V_{i,i,i,i}=\frac{1}{2(2\pi)^3}\int \mathrm{d}\boldsymbol{k}\tilde{U}_{dd}(\boldsymbol{k})\,\tilde{\rho}(\boldsymbol{k})\,\tilde{\rho}(-\boldsymbol{k}), \tag{56}$$

where the $\tilde{U}_{dd}(\boldsymbol{k})$ and $\tilde{\rho}(\boldsymbol{k})$ are the Fourier transform of the dipole-dipole potential $U_{dd}(\boldsymbol{r}_1-\boldsymbol{r}_2)=\frac{C_{dd}}{4\pi}\frac{1-3\cos^2\theta}{|\boldsymbol{r}_1-\boldsymbol{r}_2|^3}$ and the single particle density $\rho(\boldsymbol{r})=|w(\boldsymbol{r})|^2$, respectively. Thus, the parameters J, and U in Eq. (40) are then expressed as [52–54]

$$J=-\int \mathrm{d}\boldsymbol{r}w^*(\boldsymbol{r}-\boldsymbol{r}_i)\left(-\frac{\hbar^2\nabla^2}{2m}+V(\boldsymbol{r})\right)w(\boldsymbol{r}-\boldsymbol{r}_j), \tag{57}$$

$$U=g\int \mathrm{d}\boldsymbol{r}|w(\boldsymbol{r})|^4+\frac{1}{(2\pi)^3}\int \mathrm{d}\boldsymbol{k}\tilde{U}_{dd}(\boldsymbol{k})\,\tilde{\rho}(\boldsymbol{k})\,\tilde{\rho}(-\boldsymbol{k}). \tag{58}$$

Since $J_{AB}(\boldsymbol{k})$ is equal to $J_{BA}(\boldsymbol{k})$ in hypercubic lattices, we can obtain the one-particle Green's function in terms of Matsubara frequency as

$$\begin{aligned}&G^{\mathrm{inh}}(\omega_m,\boldsymbol{k})\\ &=\sum_{l=0}^{+\infty}[C_{1A}^{(0)}(\omega_m)+C_{1B}^{(0)}(\omega_m)][C_{1A}^{(0)}(\omega_m)C_{1B}^{(0)}(\omega_m)]^l[J(\boldsymbol{k})]^{2l}\\ &\quad+2\sum_{l=0}^{+\infty}[C_{1A}^{(0)}(\omega_m)C_{1B}^{(0)}(\omega_m)]^{l+1}[J(\boldsymbol{k})]^{2l+1}.\end{aligned} \tag{59}$$

Thus, with similar method to get the momentum distribution function for Bose gases in hexagonal lattice, the momentum distribution function of Bose gases in square optical lattice can in principle be calculated out analytically.

However, in order to calculate the one-particle Green's function quantitatively and to plot the corresponding time-of-flight absorption pictures, some basic facts and parameters of possible experiments need to be clarified. It is proposed [55] that the EBHM may be realized in experiment by trapping ultracold electropolar molecules RbCs (Recently, a similar EBHM is realized in experiment by using strongly magnetic erbium atoms [57]) in a cubic optical lattice created by laser beams with wavelength $\lambda=790\pm40$ nm and the corresponding s-wave

scattering length of RbCs was estimated to be about $a_s = 5.29$ nm [56]. In experiment, in order to eliminate the influence of the third dimension to reveal the 2D properties of the system, the lattice depth in the third dimension $V_3 = 30E_R$ would be a reasonable choice [46–48]. When taking into account all these possible experimental facts, the hopping parameter J and onsite repulsive interaction parameter U takes the explicit forms

$$J = E_R \left(\frac{\pi^2 - 4}{4} \widetilde{V}_0 - \frac{1}{\sqrt{\widetilde{V}_0}} \right) \mathrm{e}^{-\frac{\pi^2 \sqrt{\widetilde{V}_0}}{4}}, \tag{60}$$

and

$$U \approx E_R \sqrt{8\pi} \frac{a_s}{a} \widetilde{V}_0^{\frac{1}{2}} 30^{\frac{1}{4}} + \frac{C_{dd}}{(2\pi)^2 a^3} \sum_{n=1}^{2} \frac{1}{n!} \times \left(-\frac{\sqrt{30} - \sqrt{\widetilde{V}_0}}{2\pi^2 \sqrt{30} \sqrt{\widetilde{V}_0}} \right)^n f(n) g(n), \tag{61}$$

respectively. The notation $f(n)$ and $g(n)$ takes the explicit forms

$$f(n) = -\frac{n\pi\Gamma(1+n)}{3\Gamma(2.5+n)}, \tag{62}$$

and

$$g(n) = 2^{\frac{3n}{2}+\frac{5}{4}} 15^{\frac{n}{2}+\frac{3}{4}} \pi^{2n+3} \times \left[\Gamma\left(n + \frac{3}{2}\right) - \Gamma\left(n + \frac{3}{2}, \sqrt{\frac{2}{15}}\right) \right], \tag{63}$$

where $\Gamma(n)$ is gamma function and $\Gamma(n, m)$ is incomplete gamma function.

From Fig. 4(a) we see that when $zV < U$, there are two types of localized states, i.e., CDW states and MI states. In order to illustrate the change of the time-of-flight pictures when tuning the lattice depth to cross the phase boundaries for these two different cases, we set $zV = 0.4U$ with $\theta = \frac{\pi}{2}$ and focus on the cases of CDW(2,1) and MI(2,2) to see the time-of-flight behavior when crossing the phase boundaries. We plot our analytical results of the time-of-flight absorption pictures for these two cases in Fig. 5 and Fig. 6, respectively.

From these time-of-flight absorption pictures, we clearly see that the quantum phase transition between the CDW(2,1) state and the compressible phase surrounding it roughly happens in the region around $8.014 \leq \widetilde{V}_0 \leq 8.22$, while the quantum phase transition between MI(2,2) state and the compressible phase surrounding it is roughly around the region of $7.439 \leq \widetilde{V}_0 \leq 7.531$. Furthermore, from Fig. 4(a) together with Eqs. (60) and (61), the critical trapping potential $\widetilde{V}_0$ of CDW(2,1)-SS (MI(2,2)-SF) phase transition

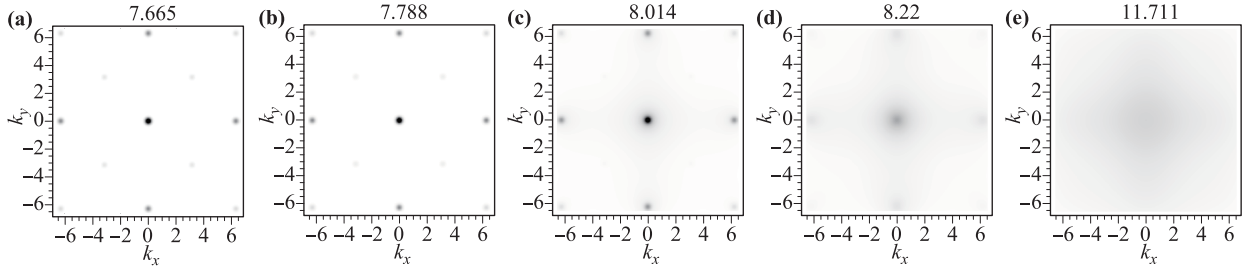

Fig. 5 At zero temperature, the generalized Green's function calculation of the time-of-flight absorption pictures for various $\widetilde{V}_0$ for an ultracold dipolar RbCs system in a square lattice with its localized state being CDW(2,1). k_x and k_y in the plots take the unit of $\frac{1}{a}$.

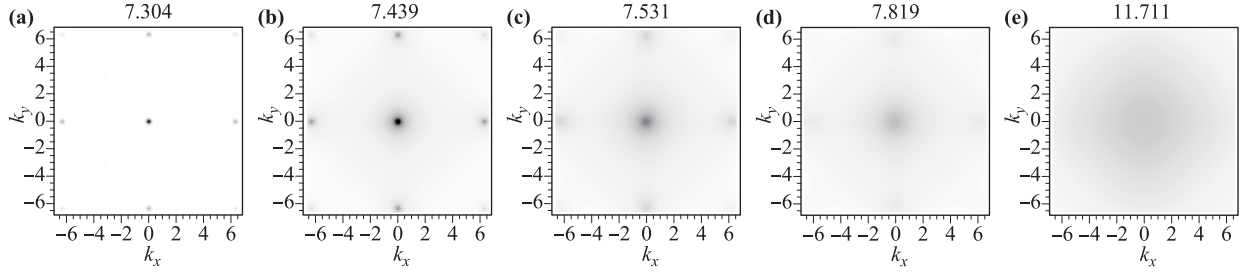

Fig. 6 At zero temperature, the generalized Green's function calculation of the time-of-flight absorption pictures for various $\widetilde{V}_0$ for an ultracold dipolar RbCs system in a square lattice with its localized state being MI(2,2). k_x and k_y in the plots take the unit of $\frac{1}{a}$.

is $\widetilde{V}_0^c = 8.085$ ($\widetilde{V}_0^c = 7.455$). The critical trapping potential $\widetilde{V}_0^c$ obtained from those two approaches is consistent with each other. When we compare the Fig. 5 with Fig. 6 carefully, we find that there are extra peaks at $(k_x, k_y) = (\pm\frac{\pi}{a}, \pm\frac{\pi}{a})$ in Figs. 5(a) and (b) (If $\widetilde{V}_0 < \widetilde{V}_0^c$, there are ghost peaks in Fig. 6(a), but no ghost peak in Figs. 5(a) and (b) [58].). This is believed to be a sort of evidence that the compressible phase surrounding the CDW phase in the phase diagram could be SS phase [59].

It should be emphasized that the results in compressible regions mentioned above are not quantitatively satisfactory because of the unphysical non-convergent nature of the Green's function in those phases, and the corresponding order parameters need to be calculated in order to get more accurate information deep in those compressible states. Since we are concerned about the particle density distribution in momentum space and only differences between regions with high and low intensity are of interest in time-of-flight measurement, meaningful results in compressible states can nevertheless be extracted qualitatively in the present manner. As we can see, the time-of-flight pictures exhibited above clearly show a notable difference between cases with shallow and deep lattice depths. The characteristic sharp peaks reflect the phase coherence in the system, indicating that the system is in a compressible state.

6 Summary

In summary, we have developed a generalized re-summed Green's function method in this paper. This generalization makes the re-summed Green's function not only a powerful tool to tackle the problems in ultracold Bose systems with homogeneous lattice structures, but also suitable for investigating the quantum critical phenomena in ultracold Bose systems with bipartite sublattice structures. Hexagonal lattice with normal Bose–Hubbard interaction and hypercubic lattice with nearest-neighbor interaction respectively represent two types of bipartite lattice systems. Through dealing with phase diagrams and time-of-flight absorption pictures of an ultracold Bose gases in these two systems, we have illustrated the generalized Green's function method in a detail way. Due to the lattice structure or nearest-neighbor repulsive interaction, the systems become inhomogeneous and are divided into two sublattices. This inhomogeneity of the lattice structure invalidates the Green's function method in old fashion. In order to resolve this problem, we have generalized the Green's function method, and have treated the cumulants on different sublattice separately during the perturbative cumulant expansion of the Green's function. The present generalization allows us to investigate the quantum phase transitions in the system between incompressible localized states (MI or CDW) and compressible delocalized phases (SF or SS). To the lowest order, we have calculated the phase diagrams of hexagonal lattice systems and hypercubic lattice systems for different nearest-neighbor interaction V. Actually, as discussed before, the lowest order re-summed Green's function is in a sense a sort of mean field theory treatment, however, from Eq. (20) we clearly see that the generalized re-summed Green's function method may in principle go beyond mean field by adding loop diagrams consisting of higher order cumulants. Moreover, according to Eqs. (29) and (47), to investigate the finite-temperature properties of the system is rather straightforward(finite temperature for hexagonal lattice have been presented in Fig. 1), but it is very difficult to obtain finite temperature phase diagrams by other methods, e.g., mean field theory [5], strong-coupling expansion [7], effective potential method [9, 10], and Gutzwiller approach [2]. In addition, with the help of the generalized Green's function method, we have calculated analytically the time-of-flight absorption pictures of ultracold Bose gases in these two types of bipartite lattices. In hexagonal lattice, the time-of-flight absorption pictures obtained by generalized Green's function method are in good qualitative agreement with the experimental data [38] and it is obtained by analytical method for the first time. In square optical lattice, the extra peaks at $(k_x, k_y) = (\pm\frac{\pi}{a}, \pm\frac{\pi}{a})$ in our result may be looked upon as a hint that the CDW state could go into a SS phase by tuning the optical lattice depth.

Acknowledgements Y.J. acknowledges Axel Pelster for his stimulating and fruitful discussions. Z.L. acknowledges inspiring discussions with Yan Chen. This work was supported by the National Natural Science Foundation of China [Grant Nos. 11074043 (Z.L.), 11274069 (Z.L.) and 11275119 (Y.J.)] and by the State Key Programs of China (Grant Nos. 2012CB921604 and 2009CB929204) (Z.L.). This work was also supported by Ph.D. Programs Foundation of Ministry of Education of China under Grant No. 20123108110004 (Y.J.).

References and notes

1. M. Greiner, O. Mandel, T. Esslinger, T. W. Hänsch, and I. Bloch, Quantum phase transition from a superfluid to a Mott insulator in a gas of ultracold atoms, *Nature* 415(6867), 39 (2002)
2. M. Lewenstein, A. Sanpera, V. Ahufinger, B. Damski, A. Sen(De), and U. Sen, Ultracold atomic gases in optical lattices: Mimicking condensed matter physics and beyond, *Adv. Phys.* 56(2), 243 (2007)
3. I. Bloch, J. Dalibard, and W. Zwerger, Many-body physics with ultracold gases, *Rev. Mod. Phys.* 80(3), 885 (2008); and the references therein.

4. S. Sachdev, Quantum Phase Transitions, Cambridge: Cambridge University Press, 1999
5. M. P. A. Fisher, P. B. Weichman, G. Grinstein, and D. S. Fisher, Boson localization and the superfluid-insulator transition, *Phys. Rev. B* 40(1), 546 (1989)
6. D. Jaksch, C. Bruder, J. I. Cirac, C. W. Gardiner, and P. Zoller, Cold bosonic atoms in optical lattices, *Phys. Rev. Lett.* 81(15), 3108 (1998)
7. J. K. Freericks and H. Monien, Strong-coupling expansions for the pure and disordered Bose–Hubbard model, *Phys. Rev. B* 53(5), 2691 (1996)
8. B. Capogrosso-Sansone, N. V. Prokof'ev, and B. V. Svistunov, Phase diagram and thermodynamics of the three-dimensional Bose-Hubbard model, *Phys. Rev. B* 75(13), 134302 (2007)
9. F. E. A. dos Santos and A. Pelster, Quantum phase diagram of bosons in optical lattices, *Phy. Rev. A* 79(1), 013614 (2009)
10. Z. Lin, J. Zhang, and Y. Jiang, Quantum phase transitions of ultracold Bose systems in nonrectangular optical lattices, *Phys. Rev. A* 85(2), 023619 (2012)
11. N. Teichmann, D. Hinrichs, and M. Holthaus, Reference data for phase diagrams of triangular and hexagonal bosonic lattices, *Europhys. Lett.* 91(1), 10004 (2010)
12. J. Zinn-Justin, Quantum Field Theory and Critical Phenomena, 3rd Ed., Clarendon Press, 1996
13. H. Kleinert and V. Schulte-Frohlinde, Critical Properties of ϕ^4-Theories, World Scientific, 2001
14. V. A. Kashurnikov, N. V. Prokof'ev, and B. V. Svistunov, Revealing the superfluid–Mott-insulator transition in an optical lattice, *Phys. Rev. A* 66, 031601(R) (2002)
15. A. Hoffmann and A. Pelster, Visibility of cold atomic gases in optical lattices for finite temperatures, *Phys. Rev. A* 79(5), 053623 (2009)
16. Z. Lin, J. Zhang, and Y. Jiang, Visibility of ultracold Bose system in triangular optical lattices, *Phys. Rev. A* 86(3), 033625 (2012)
17. W. Metzner, Linked-cluster expansion around the atomic limit of the Hubbard model, *Phys. Rev. B* 43(10), 8549 (1991)
18. M. Ohliger, Diploma thesis, Free University of Berlin, 2008
19. C. Becker, P. Soltan-Panahi, J. Kronjäger, S. Dörscher, K. Bongs, and K. Sengstock, Ultracold quantum gases in triangular optical lattices, *New J. Phys.* 12(6), 065025 (2010)
20. T. D. Graß, F. E. A. dos Santos, and A. Pelster, Excitation spectra of bosons in optical lattices from the Schwinger–Keldysh calculation, *Phys. Rev. A* 84(1), 013613 (2011)
21. T. Lahaye, C. Menotti, L. Santos, M. Lewenstein, and T. Pfau, The physics of dipolar bosonic quantum gases, *Rep. Prog. Phys.* 72(12), 126401 (2009)
22. C. Trefzger, C. Menotti, B. Capogrosso-Sansone, and M. Lewenstein, Ultracold dipolar gases in optical lattices, *J. Phys. At. Mol. Opt. Phys.* 44(19), 193001 (2011)
23. A. Lauer, D. Muth, and M. Fleischhauer, Transport-induced melting of crystals of Rydberg dressed atoms in a one-dimensional lattice, *New J. Phys.* 14(9), 095009 (2012)
24. P. Schauß, M. Cheneau, M. Endres, T. Fukuhara, S. Hild, A. Omran, T. Pohl, C. Gross, S. Kuhr, and I. Bloch, Observation of spatially ordered structures in a two-dimensional Rydberg gas, *Nature* 491(7422), 87 (2012)
25. A. Safavi-Naini, S. G. Soyler, G. Pupillo, H. R. Sadeghpour, and B. Capogrosso-Sansone, Quantum phases of dipolar bosons in bilayer geometry, *New J. Phys.* 15(1), 013036 (2013)
26. E. Altman, W. Hofstetter, E. Demler, and M. D. Lukin, Phase diagram of two-component bosons on an optical lattice, *New J. Phys.* 5, 113 (2003)
27. P. Soltan-Panahi, D. Lühmann, J. Struck, P. Windpassinger, and K. Sengstock, Quantum phase transition to unconventional multi-orbital superfluidity in optical lattices, *Nat. Phys.* 8, 71 (2012)
28. A. Eckardt, P. Hauke, P. Soltan-Panahi, C. Becker, K. Sengstock, and M. Lewenstein, Frustrated quantum antiferromagnetism with ultracold bosons in a triangular lattice, *Europhys. Lett.* 89(1), 10010 (2010)
29. S. Pielawa, E. Berg, and S. Sachdev, Frustrated quantum Ising spins simulated by spinless bosons in a tilted lattice: From a quantum liquid to antiferromagnetic order, *Phys. Rev. B* 86(18), 184435 (2012)
30. J. Ye, K. Zhang, Y. Li, Y. Chen, and W. Zhang, Optical Bragg, atomic Bragg and cavity QED detections of quantum phases and excitation spectra of ultracold atoms in bipartite and frustrated optical lattices, *Ann. Phys.* 328, 103 (2013)
31. S. Peil, J. V. Porto, B. Laburthe Tolra, J. M. Obrecht, B. E. King, M. Subbotin, S. L. Rolston, and W. D. Phillips, Patterned loading of a Bose-Einstein condensate into an optical lattice, *Phys. Rev. A* 67, 051603(R) (2003)
32. J. Sebby-Strabley, M. Anderlini, P. S. Jessen, and J. V. Porto, Lattice of double wells for manipulating pairs of cold atoms, *Phys. Rev. A* 73(3), 033605 (2006)
33. S. Fölling, S. Trotzky, P. Cheinet, M. Feld, R. Saers, A. Widera, T. Müller, and I. Bloch, Direct observation of second-order atom tunnelling, *Nature* 448(7157), 1029 (2007)
34. P. Cheinet, S. Trotzky, M. Feld, U. Schnorrberger, M. Moreno-Cardoner, S. Fölling, and I. Bloch, Counting atoms using interaction blockade in an optical superlattice, *Phys. Rev. Lett.* 101(9), 090404 (2008)
35. G. B. Jo, J. Guzman, C. K. Thomas, P. Hosur, A. Vishwanath, and D. M. Stamper-Kurn, Ultracold atoms in a tunable optical Kagome lattice, *Phys. Rev. Lett.* 108(4), 045305 (2012)

36. T. Wang, X. F. Zhang, S. Eggert, and A. Pelster, Generalized effective-potential Landau theory for bosonic quadratic superlattices, *Phys. Rev. A* 87(6), 063615 (2013)

37. M. Ohliger and A. Pelster, M. Ohliger, A. Pelster, and J. World, Green's Function Approach to the Bose-Hubbard Model, *World Journal of Condensed Matter Physics* 3, 125 (2013), arXiv: 0810.4399

38. P. Soltan-Panahi, J. Struck, P. Hauke, A. Bick, W. Plenkers, G. Meineke, C. Becker, P. Windpassinger, M. Lewenstein, and K. Sengstock, Multi-component quantum gases in spin-dependent hexagonal lattices, *Nat. Phys.* 7(5), 434 (2011)

39. M. Iskin and J. K. Freericks, Strong-coupling perturbation theory for the extended Bose-Hubbard model, *Phys. Rev. A* 79(5), 053634 (2009)

40. M. Iskin and J. K. Freericks, Momentum distribution of the insulating phases of the extended Bose-Hubbard model, *Phys. Rev. A* 80(6), 063610 (2009)

41. D. van Oosten, P. van der Straten, and H. T. C. Stoof, Quantum phases in an optical lattice, *Phys. Rev. A* 63(5), 053601 (2001)

42. B. Bradlyn, F. E. A. dos Santos, and A. Pelster, Effective action approach for quantum phase transitions in bosonic lattices, *Phys. Rev. A* 79(1), 013615 (2009)

43. M. Peskin and D. Schröder, An Introduction to Quantum Field Theory, Westview Press, Boulder, 1995

44. D. L. Kovrizhin, G. V. Pai, and S. Sinha, Density wave and supersolid phases of correlated bosons in an optical lattice, *Europhys. Lett.* 72(2), 162 (2005)

45. M. Köhl, H. Moritz, T. Stöferle, K. Günter, and T. Esslinger, Fermionic atoms in a three dimensional optical lattice: Observing Fermi surfaces, dynamics, and interactions, *Phys. Rev. Lett.* 94(8), 080403 (2005)

46. C. Becker, P. Soltan-Panahi, J. Kronjäger, S. Dörscher, K. Bongs, and K. Sengstock, Ultracold quantum gases in triangular optical lattices, *New J. Phys.* 12(6), 065025 (2010)

47. M. Köhl, H. Moritz, T. Stöferle, C. Schori, and T. Esslinger, Superfluid to Mott insulator transition in one, two, and three dimensions, *J. Low Temp. Phys.* 138(3–4), 635 (2005)

48. I. B. Spielman, W. D. Phillips, and J. V. Porto, Mott-insulator transition in a two-dimensional atomic Bose gas, *Phys. Rev. Lett.* 98(8), 080404 (2007)

49. M. Iskin, Route to supersolidity for the extended Bose-Hubbard model, *Phys. Rev. A* 83, 051606(R) (2011)

50. M. Boninsegni and N. V. Prokof'ev, Supersolids: What and where are they? *Rev. Mod. Phys.* 84(2), 759 (2012)

51. O. Dutta, M. Gajda, P. Hauke, M. Lewenstein, D.S. Lühmann, B. A. Malomed, T. Sowiński, and J. Zakrzewski, Non-standard Hubbard models in optical lattices: A review, *Rep. Prog. Phys.* 78(6), 066001 (2015)

52. M. Lewenstein, A. Sanpera, and V. Ahufinger, Ultracold Atoms in Optical Lattices: Simulating Quantum Many-Body Systems, Oxford: Oxford University Press, 2012, pp 182–183

53. K. Góral, K. Rzążewski, and T. Pfau, Bose–Einstein condensation with magnetic dipole-dipole forces, *Phys. Rev. A* 61, 051601(R) (2000)

54. K. Góral and L. Santos, Ground state and elementary excitations of single and binary Bose-Einstein condensates of trapped dipolar gases, *Phys. Rev. A* 66(2), 023613 (2002)

55. S. Kotochigova and E. Tiesinga, Controlling polar molecules in optical lattices, *Phys. Rev. A* 73, 041405(R)

56. T. Sowiński, O. Dutta, P. Hauke, L. Tagliacozzo, and M. Lewenstein, Dipolar molecules in optical lattices, *Phys. Rev. Lett.* 108(11), 115301 (2012)

57. S. Baier, M. J. Mark, D. Petter, K. Aikawa, L. Chomaz, Z. Cai, M. Baranov, P. Zoller, and F. Ferlaino, Extended Bose–Hubbard models with ultracold magnetic atoms, *Science* 352(6282), 201 (2016)

58. Disgusting ghost peaks are well known in cubic lattice systems [15]. Our method shows the existence of ghost peaks in square lattice when $J/U > (J/U)_c$, but no ghost peak in triangular [16] and hexagonal lattice for arbitrary J/U. Thus, the existence of disgusting ghost peaks is not only due to the divergence of re-summed Green' function, but also depends on the lattice structure or some unknown reasons. At the critical point ($\widetilde{V}_0 = \widetilde{V}_0^c$), the ground state of the system is neither localized phases (MI or CDW) nor compressible phases (SS or SF), but it includes characteristic fingerprints of the physical properties of both localized and compressible phases. At $\widetilde{V}_0^c$, some tiny satellite peaks appear in 'SS' phase but not in 'SF' phase. The appearance of those tiny peaks can be deemed to be an evidence of 'SS' phase, since it coincides with the feature of 'SS' phase. In the case of $J/U > (J/U)_c$, our theory may not be exactly solid, but it is available for triangular [16] and hexagonal systems. The above-mentioned argument indicates that when $J/U > (J/U)_c$, if these satellite peaks appear in SS phase, these are real peaks; but they should be taken as ghost peaks in SF phases if existing, since there is no such peaks at the critical point where our theory is valid and it also does not coincide with the features of SF phase.

59. V. W. Scarola, E. Demler, and S. Das Sarma, Searching for a supersolid in cold-atom optical lattices, *Phys. Rev. A* 73, 051601(R) (2006)